# Bridging the gap between toxicity and carcinogenicity of mineral fibres by connecting the fibre parameters to the key characteristics of carcinogens: A comprehensive model inspiring asbestos-induced cancer prevention strategies

Alessandro F. Gualtieri [a,*], Erika Ferrari [a], Luca Rigamonti [a], Barbara Ruozi [b], Serena Mirata [c,d], Vanessa Almonti [d,e], Mario Passalacqua [d,e], Stefania Vernazza [d,e], Silvia Di Valerio [f], Giovanni Tossetta [g], Salvatore Vaiasicca [f], Antonio D. Procopio [f], Francesca Fazioli [f], Daniela Marzioni [g], Armanda Pugnaloni [f], Sonia Scarfì [c,d]

[a] *Department of Chemical and Geological Sciences, University of Modena and Reggio Emilia, Modena, Italy*
[b] *Department of Life Sciences, University of Modena and Reggio Emilia, Modena, Italy*
[c] *Department Earth, Environment and Life Sciences, University of Genova, Genova, Italy*
[d] *Inter-University Center for the Promotion of the 3Rs Principles in Teaching & Research, Pisa, Italy*
[e] *Department Experimental Medicine, University of Genova, Genova, Italy*
[f] *Department of Clinical and Molecular Sciences, Polytechnic University of Marche, Torrette di Ancona, Italy*
[g] *Department of Experimental and Clinical Medicine, Polytechnic University of Marche, Torrette di Ancona, Italy*

ARTICLE INFO

ABSTRACT

*Background:* Today, many research groups in the world are struggling to fully understand the mechanisms leading to the carcinogenesis of hazardous mineral fibres, like asbestos, in view of devising effective cancer prevention strategies and therapies. Along this research line, our work attempts the completion of a model aimed at evaluating how, and to what extent, physical-crystal-chemical and morphological parameters of mineral fibres prompt adverse effects *in vivo* leading to carcinogenesis.

*Methods: In vitro* toxicology tests that deliver information on the 10 key characteristics of carcinogens adopted by the International Association for Research on Cancer (IARC) have been systematically collected for a commercial chrysotile, standard UICC crocidolite and wollastonite. The analysis of the *in vitro* data allowed us to assess the major fibre parameters responsible for alterations in the key characteristics of carcinogens for each investigated fibre and the intensity of their effect.

*Results:* Crystal habit and density of the fibres affect exposure but are not major parameters contributing to the KCs. For chrysotile, besides length, we found that fibre parameters that greatly contribute to the KCs are the surface area and the dissolution rate with the related velocity of release of metals (namely iron). For crocidolite, they are the fibre length, iron content and related parameters like the ferrous iron content, iron nuclearity, transition metals content and zeta potential.

*Conclusions:* The results of our study can be a starting point for developing personalized cancer screening and prevention strategies as long as the nature of the fibre of the exposed patient is known. We can speculate on a future personalized prevention therapy targeting the fibres with surface-engineered nanocarriers with active complexes that are selective for the surface charge of the fibres. For chrysotile, a complex with deferasirox that can chelate $Fe^{2+}$ and deferoxamine that preferentially chelates $Fe^{3+}$ is proposed with the anchorage to the silica chrysotile surface driven by aspartic acid. For crocidolite, deferiprone chelating both $Fe^{3+}$ and $Fe^{2+}$ combined with lysine to attract the silica crocidolite surface is proposed.

## Introduction

100 years ago, a medical doctor for the first time conjectured about the bio-chemical mechanisms leading to the formation of asbestos bodies (Fig. 1) in the lungs of an asbestos worker (Cooke, 1924). Dr. Cooke claimed that "… *some soluble fraction of asbestos plays a part in the formation of the asbestosis bodies, and … chemical action must play a not inconsiderable part in the production of the pulmonary fibrosis*". Much ground has been covered after a century of research to shed light on the overall mechanisms of carcinogenesis induced by asbestos (see for example, Anttila and Boffetta, 2020). However, many research groups worldwide are still working to better understand the adverse mechanisms leading to the carcinogenesis induced by the exposure to mineral fibres (Gualtieri, 2023) in the attempt to devise effective cancer prevention strategies.

According to the authors' view, there are basically three reasons to explain the difficulty encountered by scientists in finalising a solid and conclusive quantitative model elucidating these bio-chemical mechanisms. The first reason is that mineral fibres, including asbestos, are natural materials and therefore each of them is a unique entity with distinctive physical–chemical-morphological characteristics that makes its interaction with the organism singular. A general classification of mineral fibres and their behaviour *in vivo* do exist (Liddell and Miller, 1991; Gualtieri, 2017) but singularities and deviations are observed, making their behaviour *in vivo* unique and blurring any standard model. The second reason is that the concept of individuality expressed for mineral fibres can also be applied to carcinogenesis. The forms of cancer that develop as a result of the interaction between a mineral fibre agent and the organism are so complex and multifaceted that even in this case generalisation of the phenomenon is almost impossible. For example, in the case of pleural malignant mesothelioma, the typical neoplasm induced by the exposure to asbestos, the classification includes at least three major histological types (epithelioid, sarcomatoid, and biphasic) and a number of subtypes and hybrid forms (Pavlisko and Sporn, 2013; Carbone et al., 2019) whose origin is too hard to be traced back to the specific action of single mineral fibre agents. The third reason is that since at least half a century scientific data and discussion on carcinogenesis of asbestos fibres are biased and twisted by misconducts and lobbying of consultants/experts whose allegations with the asbestos industry make the general contest even more confused and the goal of drawing clear conclusive general models utopian. This issue is so true that Holmes (2013) some years ago raised the alarming question "*Does asbestos corrupt more than just DNA?*"

In this scenario, the present work is the completion of the model presented in this journal by Gualtieri (2021), aimed at evaluating how and to what extent physical-crystal-chemical and morphological parameters of mineral fibres prompt adverse effects *in vivo* leading to carcinogenesis. As described in Gualtieri (2021), the model attempts to bridge the gap between toxicity *in vitro* and carcinogenicity *in vivo* of mineral fibres and identifies the fibres' parameters that actively contribute to the key characteristics of carcinogens. The Fibre Potential Toxicity/Pathogenicity Index (FPTI) model (Gualtieri, 2018; Gualtieri,

2021) screens all the physical/crystal-chemical/morphological parameters of a mineral fibre inducing biological mechanisms responsible for adverse effects and allows the determination of the fibre toxicity/pathogenicity potential. Specifically, the fibre parameters are: morphometric (fibre length, width, crystal curvature, crystal habit, fibre density, hydrophobic character of the surface, surface area); chemical (total iron content, ferrous iron, surface ferrous iron/iron nuclearity, content of metals other than iron); biodurability-related (dissolution rate, velocity of iron release, velocity of silica dissolution, velocity of release of metals); surface activity (zeta potential, fibres' aggregation, cation exchange). The fibres induce specific adverse effects that can be measured *in vitro* with dedicated cellular or acellular toxicity tests. These measurable adverse effects are tied to *in vivo* pathological processes attributed to the characteristics of carcinogens: the 10 KCs used by IARC to evaluate the strength of the mechanistic evidence for an agent are: KC1: Is electrophilic or can be metabolically activated to electrophiles? KC2: Is genotoxic? KC3: Alters DNA repair and causes genomic instability? KC4: Induces epigenetic alterations? KC5: Induces oxidative stress? KC6: Induces chronic inflammation? KC7: Is immunosuppressive? KC8: Modulates receptor-mediated effects? KC9: Causes immortalization? KC10: Alters cell proliferation, cell death or nutrient supply? IARC reviewed all information and data of human carcinogenesis mechanisms and found that *Group 1* agents (like asbestos minerals) show one or more of the 10 KCs (Smith et al., 2016; Krewski et al., 2019). Hence, KCs are used to evaluate mechanistic evidence, within the IARC evaluations, together with human cancer epidemiological and animal cancer data, of the carcinogenic potential of an agent. It should be remarked that, with the exception of KC 5, even a single KC exhibited by an agent may result in a mechanistic evidence of carcinogenicity.

In the comprehensive model proposed here, each fibre parameter is linked to adverse effects that can be measured *in vitro* and, in turn, to the pathological processes *in vivo* attributed to the KCs. The example described in Gualtieri (2021) regards the "fibre length parameter" of a long (eventually biodurable) asbestos agent that prompts frustrated phagocytosis of macrophages (a major adverse effect whose intensity can be measured with *in vitro* toxicity test) that in turn leads to oxidative stress and chronic inflammation (major adverse effects) classified as KC 5 and KC 6. Of course, cross-correlations must be considered because, for example, chronic inflammation is due to both length of the fibres and biodurability (Donaldson et al., 2010).

Here, we present the final step of the process. Representative samples of mineral fibres have been fully characterized to determine all their physical-crystal chemical and morphological parameters. We considered two distinct batches of a commercial chrysotile sample from Ural Mountains (Russian) with short (≤5 μm) (**SC**) and long (>5 μm) (**LC**) fibres, UICC crocidolite (South Africa) (**cro**), selected as positive carcinogenic standard, and wollastonite NYAD G from Willsboro-Lewis mining district (New York, USA) (**wol**), selected as negative carcinogenic standard (Di Giuseppe et al., 2021b). For each sample, specific *in vitro* toxicity tests yielding information on the 10 KCs have been systematically measured. In this way, it is possible to determine (i) which of the 10 KCs are activated for each fibre sample (knowledge of the specific



**Fig. 1.** An optical microscopy image of outstanding historical importance showing chrysotile coating asbestos bodies (ca. 30 μm long) that exactly 100 years ago Dr. Cooke observed in the lungs of an asbestos worker who died of asbestosis (Cooke, 1924).

characteristics of cancer that are attributed a fibre species); (ii) the intensity of the KCs activated for each fibre sample; (iii) which of the fibre parameters is responsible for the activation of the KCs for each fibre sample; and (iv) cross-correlations and mutual control of the fibre parameters responsible for the activation of the KCs for each fibre sample. In the new era of precision medicine (Ye et al., 2019), this piece of information can be of inspiration for developing personalized cancer screening and prevention strategies as long as the nature of the fibre the patient was exposed to is known. In the case of carcinogenic mineral fibres, target prevention screening and strategies, usually focussed on genetic factors (Carbone et al., 2019), may be personalized also accounting for the nature of the mineral fibre carcinogen. This concept is already shared by some specialists like Toyokuni (2019) who is aware that whether the exposing asbestos fibre is iron-free or iron-rich makes a difference (Toyokuni, 2019; Motooka and Toyokuni, 2023).

## Materials and methods

### Mineral fibres

The mineral fibres used in this research project were:

(i) a commercial chrysotile sample produced by the Orenburg Minerals mine near Yasny, southern Ural Mountains (Russia). The sample is composed of clinochrysotile with minor orthochrysotile, and possibly very minor impurities of lizardite-1 T, magnetite, hydromagnesite, and calcite. The chemical formula is $(Mg_{2.870}Fe^{2+}_{0.027}Al_{0.034}Cr_{0.005}Ni_{0.006})_{2.986}(OH)_4Si_{1.92}O_5$, and the measured density is 2.58 g/cm$^3$ (Di Giuseppe et al., 2021a). The biodurability (calculated total dissolution time of 0.4 y in acidic fluid simulating the intracellular phago-lysosome medium: Di Giuseppe et al., 2021a) is low. Based on the differences for long and short chrysotile fibres observed in Gualtieri et al. (2023), two size classes of the pristine sample were obtained by cryogenic milling (Scognamiglio et al., 2021). The batch of the short ($\leq 5$ μm) chrysotile fibres (sample **SC**) displays a mean fibre length of 1.91 μm, a mean fibre width of 0.15 μm and a specific surface specific area of 30 m$^2$/g (Scognamiglio et al., 2021). The batch of the long (>5 μm) chrysotile fibres (sample **LC**) displays a mean fibre length of 29.8 μm, a mean fibre width of 0.4 μm and a specific surface specific area of 28.9 m$^2$/g (Scognamiglio et al., 2021);

(ii) a representative sample of UICC crocidolite standard (South African, NB #4173-111-3), selected as positive carcinogenic standard (sample **cro**). The sample contains minor (<1 wt%) hematite, magnetite, and quartz. The chemical formula is $Na_{2.53}Fe^{3+}_{2.19}Fe^{2+}_{1.47}Mg_{0.79}Ca_{0.02}Si_{8.06}O_{22}(OH)_2$. The sample is characterized by long fibres with mean length of 25 μm and diameter of 0.3 μm, a density of 3.35 g/cm$^3$, and a specific surface specific area of 16.1 m$^2$/g (Gualtieri et al., 2018). The fibre is highly biodurable (calculated total dissolution time of 66 y in acidic fluid simulating the intracellular phago-lysosome medium: Gualtieri et al., 2018);

(iii) a representative commercial sample of wollastonite NYAD G from Willsboro-Lewis mining district (New York, USA) (sample **wol**), selected as negative carcinogenic standard. The sample is composed of wollastonite-1A and minor calcite and displays a chemical formula of $Ca_{0.997}Fe^{2+}_{0.005}Fe^{3+}_{0.002}Mn_{0.003}Mg_{0.001}Si_{0.979}O_3$. The measured mean fibres' length and width are 46.6 μm and 3.74 μm, respectively. The density of the sample is 2.98 g/cm$^3$ and the measured specific surface area is 0.5 m$^2$/g (Di Giuseppe et al., 2021b). The biodurability (calculated total dissolution time of 0.08 y in acidic fluid simulating the intracellular phago-lysosome medium: Di Giuseppe et al., 2021b) is very low.

### Cell lines

Different cell lines were used in this project. SV40 large T antigen immortalized human mesothelial cells (MeT5A) were purchased from ATCC® (Rockville, USA). This cell line has been widely used for carcinogenic studies on mineral fibres as testified by an extensive body of literature (i.e., Ito et al., 2021; Maki et al., 2016; Cardile et al., 2007). The cells were maintained in standard culture medium represented by Roswell Park Memorial Institute (RPMI-1640) medium (Sigma-Aldrich, Milan, Italy) supplemented with 10 % foetal bovine serum (FBS) (Gibco, USA), 2 mM L-glutamine, 100U/ml penicillin and 100U/ml streptomycin (Sigma-Aldrich, Milan, Italy). The human endothelial umbilical cord continuous cell line (HECV) is used as a stable cell line of endothelial origin, as an easier alternative to endothelial primary cells, especially in co-culture setups for the study of the cellular crosstalk of inflamed tissues (i.e., Zbeeb et al., 2024; Brambilla et al., 2022). The MRC-5 human lung fibroblast primary cell line is widely used as a lung mesodermal cell type for the study of the toxicological effects of a plethora of pulmonary harmful stimuli, demonstrated by the extensive literature on the subject (i.e., Borchert et al., 2019; Laurent et al., 2021). The A549 human lung adenocarcinoma cell line is widely used as a surrogate of human alveolar cells since these cells can be induced to acquire a terminally differentiated alveolar phenotype by culture in Air-Liquid interface (ALI) conditions and is widely used in pulmonary related studies (i.e., Zhang et al., 2024; Dobrzynska et al., 2020). The human leukaemia monocytic cell line THP-1 is widely used because it can be easily differentiated into the M0, M1 and M2 phenotypes in culture and then co-cultured with a plethora of different cell types to mimic tissue specific interactions and challenged by the most varied stimuli such as infectious agents, asbestos and pollutants (Chanput et al., 2014; Li et al., 2012). HECV, MRC-5, A549 and THP-1 cells were obtained from the American Type Culture Collection (LGC Standards srl, Milan, Italy). HECV and A549 cells were cultured in high glucose DMEM with 2 mM L-glutamine (Biowest, France) supplemented with 10 % FBS, foetal bovine serum (Biowest) and penicillin/streptomycin as antibiotics (Corning Inc, Corning, NY, USA), whereas THP-1 cells were cultured in RPMI-1640 with 2 mM L-glutamine (Euroclone, Milan, Italy) supplemented with 10 % FBS (Euroclone), and the MRC-5 cell line was cultured in MEM medium (VWR International Srl, Italy) supplemented with sodium pyruvate and non-essential amino acids, 10 % FBS, (Euroclone, Italy) and penicillin/streptomycin as antibiotics (Corning). All cell lines were maintained at 37 °C in a humidified atmosphere with 5 % CO$_2$. THP-1-derived M0 macrophages were differentiated by adding 20 ng/mL phorbol-12-myristate 13-acetate (PMA, PeproTech EC, London, UK) to the culture medium of THP-1 naïve cells for 48 h.

All cell lines were initially tested for their level of sensitivity in terms of toxicity towards the mineral fibres of choice in order to establish the best concentrations to be used in the following experiments, as already explained above. Then the cell lines specifically used for the tests of each KC were chosen for their relevance in that particular KC. In detail, concerning the oxidative stress (KC 5), all cell lines were tested. For what concern genotoxicity (KC 2), alteration of DNA repair (KC 3), epigenetic alterations (KC 4), immunosuppression (KC 7), modulation of receptor-mediated effects (KC 8), and alteration of cell proliferation or cell death (KC 10), the cell lines used were mainly A549 and MeT5a, of alveolar and mesothelial origin, respectively, because from the genetic/metabolic alteration of these cell types arise cancers *in vivo* caused by the mineral fibres. Finally, regarding induction of chronic inflammation (KC 6), the two relevant cell types tested were macrophages (THP1-derived) and endothelial cells (HECV) since these cells are the major actors initiating, propagating and sustaining in the long term the inflammatory process in the lungs after fibre inhalation.

### In vitro toxicity test

*In vitro* toxicity assays to measure the characteristics of carcinogens

KCs (Smith et al., 2016) have been systematically measured for the 4 investigated mineral fibres. Most of them reflect the *in vitro* assays recommended to measure the KCs compiled from literature sources by Smith et al. (2020) but others specific experimental cell lines were selected for KC 6, KC 7, and KC 8 because they have been successfully applied in the past for mineral fibres and the interpretation of the results and comparison with old datasets was facilitated.

The cytotoxicity data have been described in previous studies (Mirata et al., 2022; Mirata et al., 2023; Gualtieri et al., 2023; Almonti et al., 2024). Experimental cell lines were plated in 96-well plates, with 10,000 cells/well for MET5A, HECV, MRC-5, and A549 or 50,000 cells/well for THP-1 derived macrophages, respectively, in complete medium. Briefly, the cytotoxicity assays of all the experimental cell lines were performed up to 72 h to assess the cell death at short-time exposure with fibres' concentrations of 100, 50 and 25 ug/mL, and up to 7 d for long time exposure with fibre concentrations from 25 to 10 ug/mL. Then, the 50 ug/mL fibre concentration was selected for short-term experiments (up to 72 h) and 10 or 25 ug/mL (depending on the sensitivity of the cell line) for the long-term experiments (from 7 to 21 d). Using these concentrations, cell survival for all fibres was always higher than 60 % at the chosen time points, usually ranging between 60 and 80 %, depending on the fibre and on the cell line. In our opinion, this strategy allowed us to ensure a concentration of fibres able to develop a minimum damage but enough stimulate cellular responses and activate the related transduction pathways.

For each experimental cell assay, tests were conducted in triplicate or quadruplicate, unless otherwise expressed in the text, and average and standard deviation calculated accordingly.

### KC 1: Is electrophilic or can be metabolically activated to electrophiles?

To get information on the electrophilic activity of the fibres, the glutathione depletion assay was applied (Rebecca et al., 2000). Glutathione was measured spectrophotometrically at 412 nm using the glutathione reductase (GR) recycling assay in the presence of 5,5-dithiobis (2-nitrobenzoic acid) (DTNB), with a calibration curve obtained with known concentrations of GSH. After fibre treatment (24 h), MeT5A and A549 cells were trypsinised, washed twice in cold PBS, and deproteinised in 1 % sulfosalicylic acid for 30 min at 4 °C. After centrifugation, the supernatant was recovered and analysed for glutathione quantification. The pellet was re-suspended with 1 M NaOH for recovery and protein quantification by the Bradford method using bovine serum albumine as standard. Data are the mean ± standard deviation of 3 independent experiment for each condition.

### KC 2: Is genotoxic?

Evaluation of the genotoxicity of the fibres was attempted using the alkaline Comet assay, performed using a commercially available kit (OxiSelect™ Comet Assay Kit). MeT5A and A549 cells were incubated the fibres at a concentration of 50 μg/mL. After 6 h, 24 h, and 48 h, cells were suspended in molten low-melting-point agarose (OxiSelect™ Comet Agarose 3 − Part No. 235002).

### KC 3: Alters DNA repair and causes genomic instability?

Genomic instability was evaluated by quantification of DNA damage induced by the mineral fibres (DNA double-strand break formation) by confocal microscopy as reported in Mirata et al. (2022), in THP-1 derived macrophages, HECV, and MeT-5A. Cells plated in eight-well Lab-Teck chambered slides and allowed to adhere overnight before treatment with 50 μg/mL mineral fibres for 24 h treatment or 25 μg/mL for 7 d treatment, respectively. At the end of incubation, cells were fixed with 4 % paraformaldehyde and stained with anti-gamma H2AX antibody (Abcam, Cambridge, UK), while nuclei were dyed with 2 μg/mL propidium iodide. Nuclei images were acquired in fluorescence mode using a using a Nikon Eclipse Ti2 confocal microscope equipped with a PLAN APO λD 60x oil objective (Amstelveen, The Netherlands). The resulting images (2.0 × digital zoom) were obtained acquiring the green

fluorescence of DNA double-strand breaks and the red fluorescence of propidium iodide-stained nuclei (emission range of 500–550 nm and 600–670 nm, respectively).

### KC 4: Induces epigenetic alterations?

MiRNA expression levels of miR-222 and miR-126 were evaluated for the MeT5a and A549 cells in contact with the fibres for 6 h. MiRNAs first-strand cDNA was synthetized using the TaqMan miRNA Assay (Applied Biosystems, Life Technologies) according to the manufacturer's instructions. The qRT-PCR reactions were carried out using the TaqMan® Fast Advanced Master gene expression kit (Applied Biosystems, Life Technologies) at the following conditions: 50 °C for 2 min, 95 °C for 20 s, 40 cycles of 95 °C for 1 s and 60 °C for 20 s, 4 °C. U6 RNA was used for the normalization.

Dnmt1 (DNA methyltransferase 1) expression alteration in the MeT5a and A549 cells in contact with the fibres for 24 h was measured by qPCR assay. Total RNA was retrotranscribed using the high-capacity cDNA reverse transcription kit (Applied Biosystems). The qPCR assay was performed using Realplex Mastercycler epgradient S (Eppendorf). Results were expressed as relative level $(2 − \Delta CT)$ and fold change ($2$-$\Delta\Delta CT$).

### KC 5: Induces oxidative stress?

ROS production and induced cell oxidative stress were measured using the fluorescent probe, H2DCFDA (Carboxy-H2DCFDA-C400, Invitrogen). The H2DCFDA crossing the plasma membrane of the cell, is de-acetylated to H2DCF producing a fluorescent product, DCF. THP-1, HECV, MeT5A and A549 cells were cultured for 24 h before the treatment with the fibres. Different times in the same culture medium with the fibres were used. At the end of each time points, cells were trypsinized, centrifuged for 5 min, washed twice with PBS and incubated for 30 min in the dark at 37 °C in PBS containing 10 μM (work solution) of Carboxy-H2DCFDA (1 mM) probe for 30 min at 37 °C in the dark. After the incubation the reaction was stopped with 1 ml of filtered PBS followed by centrifuged at 500*g* for 7 min. The supernatant was then removed, and the cells re-suspended in 200 μl of filtered PBS. The cells were stained with 4 μl of 10 μg/ml Propidium Iodide (PI) to exclude dead cells from the counts. Fluorescence intensity was measured using flow cytometry (Guava® easy Cyte™ Flow Cytometer; Millipore) with excitation at 488 nm. Emissions were recorded using the green channel for Carboxy-H2DCFDA and the red channel for the PI. Mean Fluorescence Intensity (MFI) was recorded on an average of 10,000 events from each sample. The results of the experiments were analysed by FlowJo software. Results were expressed as mean values ± standard deviation of fluorescence intensity.

### KC 6: Induces chronic inflammation?

To evaluate endpoints that could be linked to chronic inflammation, the mineral fibres were added to THP-1-derived macrophages and HECV endotheliocytes at a final concentration of 50 μg/mL for different times (7d and 12-14d). The gene expression profile of interleukin-1β (IL-1β), interleukin-6 (IL-6), interleukin-8 (IL-8), tumour necrosis factor-alpha (TNF-α) and monocyte chemoattractant protein-1 (MCP-1), was evaluated by qPCR relative to untreated cells. For the HECV endotheliocytes, the gene expression of transforming growth factor-β 2 (TGF-β2), intercellular adhesion molecule-1 (ICAM-1), fibronectin (FIBRO), alpha-smooth muscle actin (α-SMA), collagen 1A (COL-1A) and matrix metalloproteinase-9 (MMP-9) was also evaluated by qPCR relative to untreated cells. Total RNA was extracted using the NucleoSpin RNA, Mini kit (MACHEREY-NAGEL, Dueren, Germany). The cDNA was synthesised from 1 μg of RNA by using an iScript cDNA Synthesis Kit (Bio-Rad Laboratories, Milan, Italy). qPCR reactions were performed using the 4 × master mix (biotechrabbit GmbH, Henningsdorf, Germany). Data analyses were obtained using the DNA Engine Opticon® 3 Real-Time Detection System Software program (3.03 version), Results were expressed as relative level $(2 − \Delta CT)$ and fold change ($2$-$\Delta\Delta CT$) as

compared to CTRL.

Cytokine release of the MeT5a, A549, and THP1 cells in contact with the fibres for 24 and 48 h were measured using the Bio-Plex Pro Human Cytokine Screening Panel 11plxX (Bio-Plex, Laboratories, Milano, Italy). Luminex multiplex panel technology was used for simultaneous measurement of a panel of the following analytes: IL6, IL-8, MCP1 (Monocyte Chemoattractant Protein 1) and RANTES. Briefly, 50 µL of diluted samples and reaction standards were added, in duplicate, to a 96 multi-well plate containing analyte beads followed by incubation for 30 min at room temperature. After washing, the biotinylated antibody reporter was added and incubated for 10 min with streptavidin phycoerythrin. The levels of the cytokines were determined using the Bio-Plex array reader (Luminex, Austin, TX). The Bio-Plex Manager software optimized the standard curves automatically and returned the reading data as Median Fluorescence Intensity (MFI) and concentration (pg/mL).

The alteration of gene expression profile of growth factors TNF-α, VEGF, and TGF-β2 was evaluated in THP-1-derived macrophages, HECV endotheliocytes, and MET5a by qPCR relative to untreated cells at different times (24 h, 3d, 7d, and 14d), as already described in the previous paragraphs. The primer pairs used in all qPCR experiments, reported in the Supplementary Material 1, were designed using the Beacon Designer 7.0 software (Premier Biosoft International, Palo Alto, CA, USA) and obtained from TibMolBiol (Genova, Italy).

### KC 7: Is immunosuppressive?

To get information related to the immunosuppressive activity of the fibres, tests were performed over extended durations of exposure. MeT5a cells or THP-1 cells (differentiated towards M0 macrophages) were plated in 6-well plates at 500,000 cells/well before incubation with 10 µg/mL of mineral fibres for 7, 14 and 21 d. For all experimental conditions, the gene expression profile of anti-inflammatory mediator interleukin-10 (IL-10) was evaluated by qPCR relative to untreated cells as already described in the previous paragraph.

We also performed Bio-Plex Human Cytokine Assays, informative for the evaluation of immunosuppression, using MeT5A and A549 cell lines. The production of molecules synthesized by the cell and released into the supernatant was measured. In this case, we evaluated the suppression of production of pro-inflammatory cytokines Il-6, Il-8, MCP1 (Monocyte Chemoattractant Protein 1), and RANTES (Regulated on Activation normal T-cell expressed and secreted) in Met5A and A549 cells treated for 24 h. Luminex multiplex panel technology for simultaneous measurement of different analytes including cytokines in 96-well Bio-Rad was used.

### KC 8: Modulates receptor-mediated effects?

To evaluate the transcriptional modifications regarding Epithelial-to-Mesenchymal transition (EMT) and fibrosis, induced by the exposure to mineral fibres, MeT-5A cells were plated at 50,000 cells/well in 6-well plates and allowed to adhere overnight. Then, they were treated with the fibres (25 µg/mL final concentration) for different times (24 h, 72 h, 7 d, 14 d, or 21 d). For all experimental conditions, the gene expression of several proteins and transcription factors contributing to EMT, was evaluated by qPCR as already described in the previous paragraphs. The investigated genes were alpha-smooth muscle actin (α-SMA), fibronectin (FIBRO), matrix metalloproteinase-1 (MMP-1), matrix metalloproteinase-3 (MMP-3), Mesothelin, N-cadherin, TGF-β2, TWIST family bHLH transcription factor 1 (TWIST1), and zinc finger E-box binding homeobox 2 (ZEB2). Values were normalised to the HPRT-1 housekeeping gene mRNA expression.

### KC 9: Causes immortalization?

This KC was not tested because, as it was explained in Table 3 of Gualtieri (2021), to the knowledge of the authors, there are no data in the existing literature about the physical-crystal-chemical and morphological parameters of mineral fibres prompting adverse effects *in vivo* linked to immortalization. Hence, the correlation of the fibre

parameters to this KC cannot be done.

### KC 10: Alters cell proliferation, cell death or nutrient supply?

Cdk1 (Cyclin Dependent Kinase 1) gene expression alteration in MeT5a and A549 cells in contact with the fibres for 24 h was measured by qPCR assay. Total RNA was retrotranscribed using high-capacity cDNA reverse transcription kit (Applied Biosystems). The qPCR assay was performed using Realplex Mastercycler epgradient S (Eppendorf). Results were expressed as relative level $(2 - \Delta CT)$ and fold change $(2-\Delta\Delta CT)$ as compared to CTRL.

Alteration of cell-cycle progression was analysed by flow cytometry in MeT5a and A549 cells exposed to the fibres for 48 h, as already described in paragraph 3 (Alteration of DNA repair and genomic instability).

Table 1 reports all the *in vitro* cellular end points associated to KCs investigated in this study.

### Data reduction and application of the model

In this section we explain in detail the rationale used to develop the model. The full calculation data sheet printed as excel or PDF format is available as Supplementary Material 2. Each replicate data set of *in vitro* tests related to a KC (*e.g.* gluthathione depletion assay for MeT5A for 24 h for KC 1: line 3 in Supplementary Material Table 2) delivers single values for the 4 investigated fibres f (short chrysotile **SC**, long chrysotile **LC**, crocidolite **cro** and wollastonite **wol**). For each test, the measured

**Table 1**

*In vitro* cellular end points investigated associated to the KCs.

| KCs | End point investigated | Experimental cell line |
|---|---|---|
| 1 Is electrophilic or can be metabolically activated to electrophiles? | – Gluthathione depletion assay | MeT5a, A549 |
| 2 Is genotoxic? | – Comet assay | MeT5a, A549 |
| 3 Alters DNA repair and causes genomic instability? | – gH2AX nuclear foci count | THP-1, HECV, MET5a |
| 4 Induces epigenetic alterations? | – Altered Dnmt1 expression | Met5a, A549 |
| | – Altered miRNA expression | MeT5a, A549 |
| 5 Induces oxidative stress? | – ROS production | THP-1, HECV, MeT5a, A549 |
| | – Oxidized/reduced Glutathione ratio | MeT5a, A549 |
| 6 Induces chronic inflammation?* | Alteration of gene expression: | THP-1, HECV, HECV |
| | – IL1b, IL-6, IL-8, TNF-a, MCP1 | |
| | – TGF-b2, ICAM-1, FIBRO, a-SMA, COL-1A, MMP-9 | |
| | Cytokine release:IL-6, MCP1, RANTES | MeT5a, A549, THP-1 |
| 7 Is immunosuppressive?* | – IL-10 expression | THP-1, MeT5a, A549 |
| | – Multiplex analysis Bio-Plex Pro Human Cytokine Screening Panel 11plx X: IL-6, IL-8, MCP1, RANTES | MeT5a, A549 |
| 8 Modulates receptor-mediated effects?* | – EMT marker gene expression: | MET5a |
| | a-SMA, FIBRO, MMP-1, MMP-3, Mesothelin, N-cadherin, TGF-b2, TWIST-1, ZEB2 | |
| 9 Causes immortalization? | – | – |
| 10 Alters cell proliferation, cell death or nutrient supply? | – Alteration of cell cycle progression | MeT5a, A549 |
| | – Cdk1 altered expression | MeT5a, A549 |
| | – Growth factor altered gene expression: | THP-1, HECV, MeT5a |
| | – TNF-a, VEGF, TGF-b2 | |

* Experimental cell lines other than those suggested by Smith et al. (2020) were used. For all the other KCs, the experimental cell lines follow the protocol suggested by Smith et al. (2020).

value $x_{i,wol}$, $x_{i,SC}$, $x_{i,LC}$, $x_{i,cro}$ is subtracted from the measured value of the control. The residual values are divided by 100. The mean values $\overline{X}_{wol}$, $\overline{X}_{SC}$, $\overline{X}_{LC}$, and $\overline{X}_{cro}$ are calculated for each fibre f. Outliers are calculated using the Interquartile Range (IQR) method (Moore and McCabe, 1999) and eventually removed so that the mean value $\overline{X}_f$ can be recalculated. The obtained mean values $\overline{X}_{KCi,wol}$, $\overline{X}_{KCi,SC}$, $\overline{X}_{KCi,LC}$, and $\overline{X}_{KCi,cro}$ are normalized with respect to the greater mean value. In this way, the mean normalized *in vitro*-tested contribution of each fibre to each of the 10 KCs is calculated.

Next step was to link the fibre parameters to the pathological processes exhibited by human carcinogens. Following the conceptual scheme described in Gualtieri (2021), each specific fibre' parameter can be linked to the major adverse effects (measured from the *in vitro* toxicity tests) that reflect the 10 KCs. These relationships are fully described in Table 3 of Gualtieri (2021). For example, KC 1 is linked to the following fibre parameters: length (1,1), surface area (1,7), total iron content (1,8), ferrous iron (1,9), surface iron (1,10), content of metals (1,11), dissolution rate (1,12), velocity of release of iron (1,13), silica (1,14) and metals (1,15). For each fibre, we estimated the parameters linked to that KC. For example, only (1,1), (1,12) and (1,14) fibre parameters of wollastonite (**wol**) are linked to KC 1 because wollastonite virtually does not contain iron nor metals and its surface area is small. For each active fibre parameter of the 4 fibres, we assign the value of the normalized means $\overline{X}_{KCi,f}$, that is, 0.85 for (1,1), 0.85 for (1,12) and 0.85 for (1,14) for **wol** (lines 8, 15 and 17 in Supplementary Material Table 2, respectively). All the values of a fibre parameter (1,1 for example) linked to every KCs are summed up to assess the actual overall contribution of that fibre parameter to the KCs (columns T to V, lines 19–37 in Supplementary Material Table 2). The flow chart depicted in Fig. 2 describes the general case (left) and an example of the calculation for the fibre parameter (1,1) for **wol**.

## Results

Fig. 3A and Table 2 report the sum of the mean normalized *in vitro*-tested contribution to each KC for the 4 investigated fibres. This sum is an estimate of the overall toxicity *in vitro* of the fibres with a trend that is comparable to the values predicted by the Fibre Potential Toxicity/Pathogenicity Index (FPTI) (Gualtieri, 2018; Gualtieri, 2021).
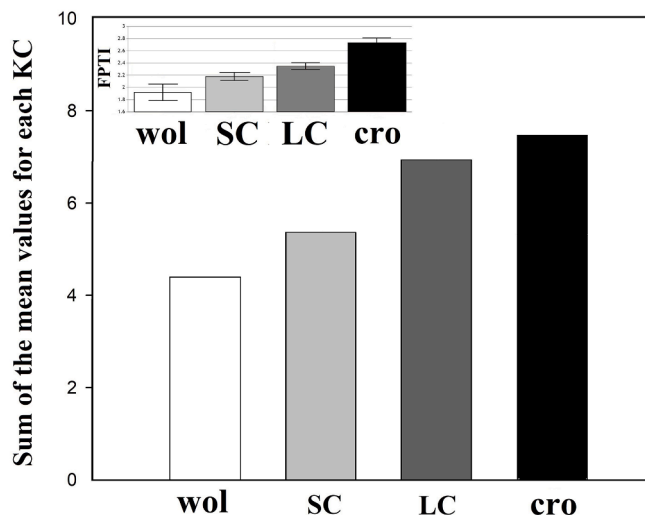


**Fig. 3A.** Sum of the mean normalized *in vitro*-tested contribution to each of the 10 KCs for the 4 investigated fibres. Legend: wol = non-carcinogenic reference wollastonite NYAG D; SC = short fibre (≤5 μm) Russian chrysotile; LC = long fibre (>5 μm) Russian chrysotile; cro = carcinogenic reference UICC crocidolite. The top left inset reports the predicted toxicity/pathogenicity potential calculated for the fibres using the FPTI model (Gualtieri, 2018).

Specifically, the FPTI values (calculated online using WebFPTI at http://fibers-fpti.unimore.it/FPTI/ref: Gualtieri et al., 2021) are: 1.917 (0.136) for the non-carcinogenic standard wollastonite NYAG D (**wol**), 2.18 (0.065) for the Russian short (≤5 μm) chrysotile fibre (**SC**), 2.35 (0.054) for the Russian long (>5 μm) chrysotile fibre (**LC**), and 2.733 (0.08) for the carcinogenic standard UICC crocidolite (**cro**). In agreement with our previous findings (Gualtieri et al., 2023), the figure clearly shows that (i) the chrysotile fibres are more toxic *in vitro* than those of wollastonite; (ii) the toxicity *in vitro* of the chrysotile fibres is lower than that of crocidolite; (iii) the toxicity *in vitro* of the short chrysotile fibres is lower than that of long chrysotile fibres. The calculation of the mean values with standard deviations and variances are reported in Table 2. The scatter of the data reflects in rather large standard deviations and variances of the mean values (in the range
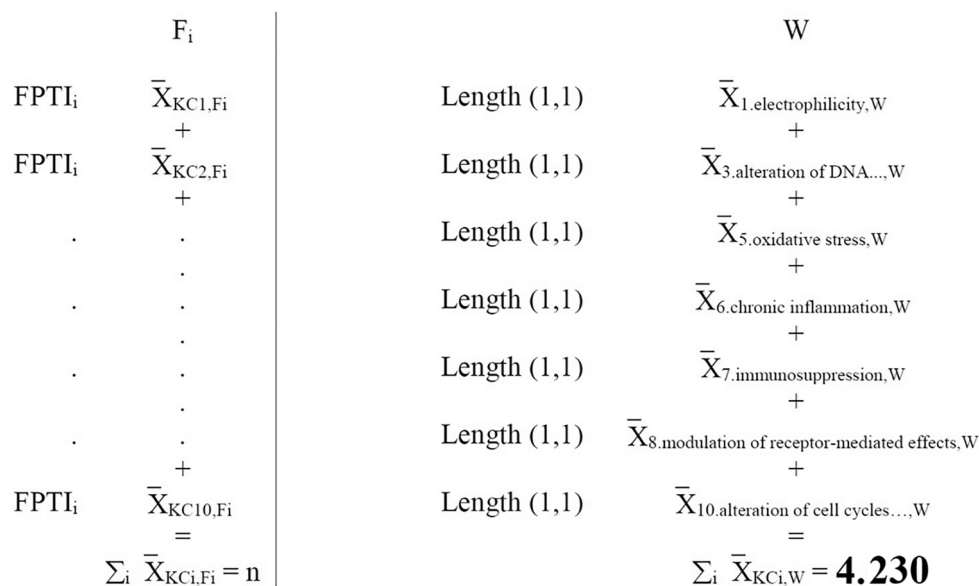


**Fig. 2.** Flow chart to explain the calculation of the sum of the contributions of the 18 fibre characteristics [(1,1) to (1,18)] active for the KCs of the 4 analysed fibres. The left side shows the general case while the right side shows an example of the calculation for the fibre parameter length (1,1) for the fibre wollastonite (wol). See text and Supplementary Material Table 2 for details.

**Table 2**

Sum of the mean normalized *in vitro*-tested contribution to each of the 10 KCs for the investigated fibres. Legend: **wol** = non-carcinogenic reference wollastonite NYAG D; **SC** = short fibre (≤5 μm) Russian chrysotile; **LC** = long fibre (>5 μm) Russian chrysotile; **cro** = carcinogenic reference UICC crocidolite. See text for details.

| KCs | wol | SC | LC | cro |
|---|---|---|---|---|
| 1 Is electrophilic or can be metabolically activated to electrophiles? | 0.850 | 0.667 | 0.867 | 1.000 |
| 2 Is genotoxic? | 0.221 | 0.365 | 0.605 | 1.000 |
| 3 Alters DNA repair and causes genomic instability? | 0.065 | 0.613 | 1.000 | 0.900 |
| 4 Induces epigenetic alterations? | 0.068 | 0.347 | 1.000 | 0.428 |
| 5 Induces oxidative stress? | 0.643 | 0.398 | 0.857 | 1.000 |
| 6 Induces chronic inflammation? | −0.276 | 0.392 | 0.114 | 1.000 |
| 7 Is immunosuppressive? | 1.000 | 0.941 | 0.817 | 0.665 |
| 8 Modulates receptor-mediated effects? | 0.948 | 1.000 | 0.761 | 0.781 |
| 9 Causes immortalization? | – | – | – | – |
| 10 Alters cell proliferation. cell death or nutrient supply? | 1.000 | 0.684 | 0.968 | 0.751 |
| Sum | 4.518 | 5.401 | 6.988 | 7.524 |
| mean | 0.452 | 0.541 | 0.698 | 0.752 |
| Standard deviation of the mean | 0.486 | 0.301 | 0.360 | 0.324 |
| Variance of the mean | 0.213 | 0.082 | 0.116 | 0.095 |

**Table 3**

Sum of the contribution of each of the 18 fibre characteristics active for the 10 KCs for the investigated fibres. Legend: **wol** = non-carcinogenic reference wollastonite NYAG D; **SC** = short fibre (≤5 μm) Russian chrysotile; **LC** = long fibre (>5 μm) Russian chrysotile; **cro** = carcinogenic reference UICC crocidolite. See text for details.

| Fibre parameter | wol | SC | LC | cro |
|---|---|---|---|---|
| Length (1.1) | 4.230 | | 4.443 | 7.525 |
| Width (1.2) | | 1.684 | 1.729 | 1.532 |
| Crystal surface (1.3) | | 1.684 | 1.729 | |
| Crystal habit (1.4) | | | | |
| Density (1.5) | | | | |
| Hydrophilicity (1.6) | 2.672 | 3.02 | 2.659 | 3.197 |
| Surface area (1.7) | | 5.406 | 6.122 | |
| Total iron content (1.8) | | | 0.867 | 7.525 |
| Ferrous iron (1.9) | | 2.625 | 2.545 | 7.525 |
| Surface ferrous iron (1.10) | | 3.016 | 3.526 | 7.525 |
| Content of metals (1.11) | | 5.406 | 6.122 | 7.525 |
| Dissolution rate (1.12) | 2.502 | 3.721 | 5.260 | |
| Velocity of iron release (1.13) | | 5.406 | 6.122 | |
| Velocity of silica formation (1.14) | 1.714 | 1.429 | 2.329 | |
| Velocity of release of metals (1.15) | | 5.406 | 6.988 | |
| Zeta potential (1.16) | | | | 4.328 |
| Aggregation (1.17) | | 1.332 | 0.930 | 1 |
| Cation exchange (1.18) | – | – | – | – |

0.301–0.486 and 0.008–0.213, respectively). A statistical analysis was performed with the Kruskal-Wallis test (Vargha and Delaney, 1998) using the online application available at http://www.statskingdom.com/kruskal-wallis-calculator.html. The results of the tests are provided as Supplementary Material 3. The Kruskal-Wallis test indicated that there is a non-significant difference in the dependent variable between the different groups, $\chi^2(3) = 6.97$, p = 0.073, with a mean rank score of 14.78 for Group1(**wol**), 12.56 for Group2 (**SC**), 22.31 for Group3 (**LC**), 22.83 for Group4 (**cro**). It should be remarked that the values of the sum allow to confirm the rank of the fibre potential toxicity delivered by the FPTI model (see Fig. 3A).

Fig. 3B reports the mean normalized *in vitro*-tested contribution to each of the 10 KCs for the 4 investigated fibres (see Table 2).The sum of the contribution of each of the 18 fibre parameters active for the 10 KCs calculated for the 4 analysed fibres is reported in Table 3. Fig. 4A plots the results of the calculation. It is clear from the figure that crystal habit (1,4) and fibre density (1,5) have no significance. Ion exchange (1,18) is also inadequate for these fibres because it applies to zeolite phases only. The irrelevance of crystal habit and fibre density in activating the KCs is due to the fact that these physical parameters determine the probability
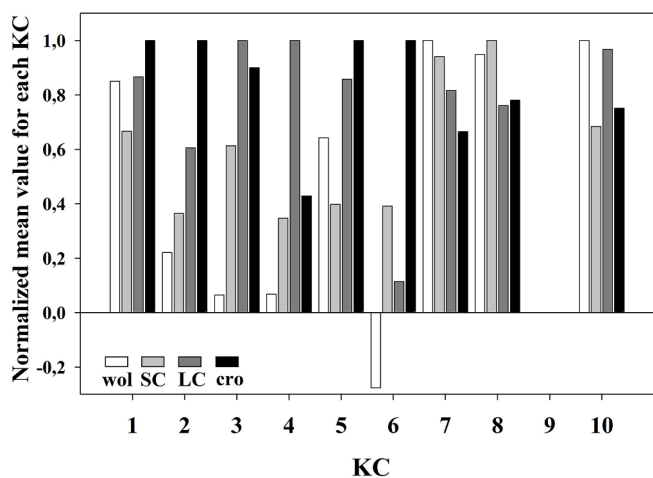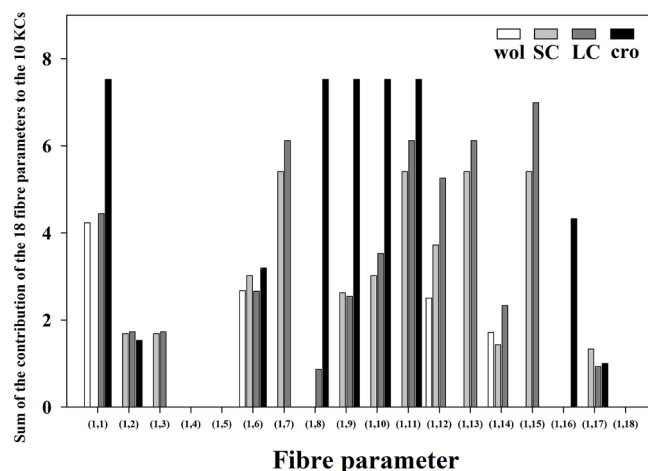


**Fig. 4A.** Sum of the contributions of the 18 fibre characteristics [(1,1) to (1,18)] active for the 10 KCs for the 4 analysed fibres, calculated according to the flow chart depicted in Fig. 2. Legend: **wol** = non-carcinogenic reference wollastonite NYAG D; **SC** = short fibre (≤5 μm) Russian chrysotile; **LC** = long fibre (>5 μm) Russian chrysotile; **cro** = carcinogenic reference UICC crocidolite. See text for details.

of the fibres to reach the lung environment but not the interaction itself with the cells and thus the possibility to activate mechanisms of carcinogenesis. The crystal habit (if a fibre is curled or needle-like) rules the depositional behaviour of the fibre once inhaled. Compared to needle-like fibres like amphiboles, curled ones such as chrysotile tend to be deposited in the upper airways, particularly at bronchial or bronchiolar bifurcations (Harris and Timbrell, 1977). At the same time, fibre density determines the aerodynamic diameter of a fibre and the depth of deposition of inhaled particles in the airways (Yeh et al., 1976).

Fig. 4B is the plot of the differences (Δ) of the sum of the contributions of the fibre parameters to the KCs $\overline{X}_{KCi,Fi}$ subtracted from the value of the non-carcinogenic standard wollastonite (**wol**) $\overline{X}_{KCi,wol}$. Specifically the light grey bars refer to the difference between the short and long chrysotile fibres $\Delta_{SC-LC} = \sum_i \overline{X}_{KCi,SC} - \sum_i \overline{X}_{KCi,LC}$, the grey bars refer to the difference between the short chrysotile fibres and crocidolite $\Delta_{SC-cro} = \sum_i \overline{X}_{KCi,SC} - \sum_i \overline{X}_{KCi,cro}$, and the dark grey bars refer to the difference
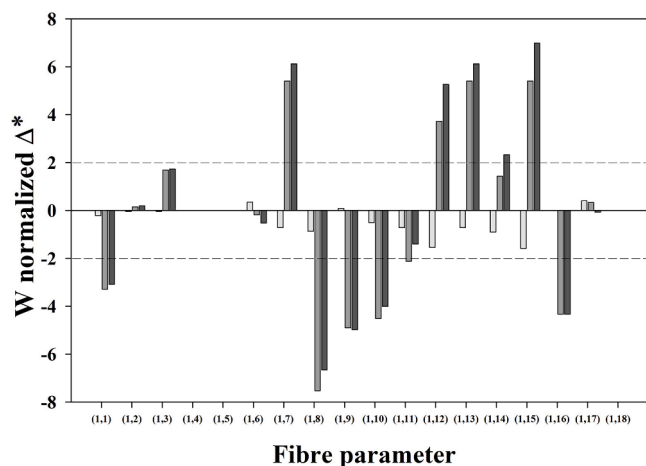


**Fig. 3B.** KCs-related normalized mean values from the *in vitro* toxicity tests for the investigated fibres. Legend: **wol** = non-carcinogenic reference wollastonite NYAG D; **SC** = short fibre (≤5 μm) Russian chrysotile; **LC** = long fibre (>5 μm) Russian chrysotile; **cro** = carcinogenic reference UICC crocidolite.

**Fig. 4B.** Plot of the differences (Δ) of the sum of the contributions of the fibre characteristics to the KCs $\overline{X}_{KCi,Fi}$ subtracted from the value of the non-carcinogenic standard wollastonite (**wol**) $\overline{X}_{KCi,wol}$. Legend: light grey = difference between the short (**SC**) and long chrysotile (**LC**) fibres $\Delta_{SC-LC}=\sum_i\overline{X}_{KCi,SC} - \sum_i\overline{X}_{KCi,LC}$; grey = difference between the short chrysotile fibres and crocidolite $\Delta_{SC-cro}=\sum_i\overline{X}_{KCi,SC} - \sum_i\overline{X}_{KCi,cro}$; dark grey = difference between the long chrysotile fibres and crocidolite (**cro**) $\Delta_{LC-cro}=\sum_i\overline{X}_{KCi,LC} - \sum_i\overline{X}_{KCi,cro}$. The thin dotted lines in the plot mark the values <|2.0| to highlight the most significant differences among the fibres.

between the long chrysotile fibres and crocidolite $\Delta_{LC-cro}=\sum_i\overline{X}_{KCi,LC} - \sum_i\overline{X}_{KCi,cro}$. The thin dotted lines in the plot are intended to be a filter for the values <|2.0| so that the most significant differences among the fibres are evidenced. Figs. 4A and 4B show that some fibre parameters do not significantly contribute to the KCs. These parameters are: fibre width (1,2), crystal curvature (1,3), crystal habit (1,4), fibre density (1,5), hydrophobic character of the surface (1,6), velocity of silica formation (1,14), fibres' aggregation (1.17), and cation exchange (1,18). The latter is an obvious result because it applies to zeolite fibres only. Of significant contribution to the KCs are: fibre length (1,1), surface area (1.7), total iron content (1.8), content of ferrous iron (1.9), surface ferrous iron (1.10), content of metals (1.11), dissolution rate (1.12), velocity of iron release (1.13), velocity of release of metals (1.15), and zeta potential (1.16).

## Discussion

Human carcinogens usually, but not always (Goodman et al., 2018), exhibit one or more KCs (Smith et al., 2020) and are used to evaluate mechanistic evidence of the carcinogenic potency of an agent classified by the IARC. If we look at the normalized mean toxicity values for each of the KCs (Fig. 3B), we can infer some important conclusions for mineral fibres. With the premise that KC 9 is not considered here, for the standard carcinogenic crocidolite (**cro**), all the KCs except for KC 4 are active with intense *in vitro* KCs-related toxicity activity. For the non-carcinogenic wollastonite standard (**wol**), 3 KCS are not active (KC 3, KC 4, and KC 6). In general, chrysotile displays intermediate cases with significant activity for all the KCs but less intense than crocidolite (**cro**). Chrysotile with short fibres (**SC**) displays lower values for KC 2, KC 4, KC 5 and KC 6 while chrysotile with long fibres (**LC**) displays high intense *in vitro* KCs-related toxicity activity.

It is noted that, according to the IARC evaluation protocols, our results determine a strong mechanistic evidence of carcinogenicity even for the non-carcinogenic wollastonite, indicating that great care must be taken in translating the evidence for the activity of these parameters into absolute parameters of carcinogenicity.

The sum of the contribution of the fibre parameters to the toxicity parameters related to the KCs is plotted in Fig. 4A. To enucleate the fibre

parameters that mostly affect carcinogenicity and possible distinctions between crocidolite and chrysotile, we have plotted the differences of the sum of the contributions of the fibre parameters to the KCs (Fig. 4B). The thin line at values <|2| permits to highlight the most significant parameters with respect to "background values". The major fibre parameters contributing to the KCs are: length (1,1), surface area (1,7); iron content (1,8), ferrous iron content (1,9), iron nuclearity (1,10), content of metals other than iron (1,11), dissolution rate (1,12), velocity of iron release (1,13), velocity of release of metals (1,15), and zeta potential (1,16). If we consider the rank and cross-correlations described in detail in Gualtieri (2018) and Mossman and Gualtieri (2020), the parent parameters are: length (1,1), iron content (1,8), content of metals (1,11), dissolution rate (1,12), and zeta potential (1,16). Descendant parameters of lower rank are: surface area (1,7) that depends on the fibre size; ferrous iron content (1,9) that depends on the iron content; iron nuclearity (1,10) that depends on iron-related parameters; velocity of iron release (1,13) and velocity of release of metals (1,15) that depend upon the dissolution rate.

The fibres size, represented by the length (1,1), and biodurability, represented by the dissolution rate (1,12), are the backbones of the "fibre toxicity paradigm" for which long, thin, and biodurable "asbestos" fibres reach the alveolar and pleural/peritoneal spaces where they induce chronic frustrated phagocytosis and inflammation (Dunningan, 1984; Donaldson et al., 2010). The negative difference between the short chrysotile fibres and crocidolite $\Delta_{SC-cro}$ (grey bars in Fig. 4B) and between the long chrysotile fibres and crocidolite $\Delta_{LC-cro}$ (ref bars in Fig. 4B) indicates that the length of crocidolite fibres has a stronger impact on the KCs than the length of chrysotile fibres. Oppositely, because chrysotile is non-biodurable and crocidolite is biodurable (Hume and Rimstidt, 1992; Gualtieri et al., 2019b), the difference between the short chrysotile fibres **SC** and crocidolite $\Delta_{SC-cro}$ and between the long chrysotile fibres **LC** and crocidolite **cro** $\Delta_{LC-cro}$ is positive (dark grey bars in (1,12), Fig. 4B). Fibre width (1,2) should not be overlooked as it defines the World Health Organization (WHO) counting criteria of respirable particles ("any elongated inorganic particle having length ≥ 5 μm, width ≤ 3 μm, and length/diameter ratio ≥ 3:1": WHO, 1997). However, it is not a major parameter here because, like the crystal habit (1,4) and density (1,5), it affects the aerodynamics of a fibre and the depth of deposition in the airways (Yeh et al., 1976) but not the interaction with the cells in the lung environment where local chronic inflammation due to alveolar macrophages' frustrated phagocytosis (Donaldson et al., 2010) is mostly determined by the fibre length. Stanton et al. (1981) first postulated that "asbestos" pathogenicity is related to biodurable fibres with length >10 μm because clearance via phagocytosis is only possible if fibre length is <10 μm as macrophages can efficiently engulf particles of that size or smaller (Donaldson et al., 2010).

The distinct crystal-chemistry of chrysotile and crocidolite explains the differences in the other parent parameters relevant for KCs. The positive zeta potential (1,16), the "electrical double layer" around a particle (Pollastri et al., 2014), of chrysotile with respect to the negative zeta potential of crocidolite explains the difference between the short chrysotile fibres **SC** and crocidolite **cro** $\Delta_{SC-cro}$ (grey bars in Fig. 4B) and between the long chrysotile fibres **LC** and crocidolite **cro** $\Delta_{LC-cro}$ (dark grey bars in Fig. 4B). Zeta potential influences the fibres' haemolytic potential, ROS production, fibre encapsulation and agglomeration known to induce biological responses (Pollastri et al., 2014). In this regard, chrysotile is known to cause hemolysis (Jiang et al., 2012) and this is also a major factor of carcinogenicity because red blood cells are rich in iron as haemoglobin, harbouring as much as 60 % of the body's iron (~4 g). The lower content of iron (1,8) and metals (1,11) in chrysotile with respect to crocidolite (Pollastri et al., 2015) explains the negative difference between the short chrysotile fibres **SC** and crocidolite **cro** $\Delta_{SC-cro}$ (grey bars in Fig. 4B) and between the long chrysotile fibres **LC** and crocidolite **cro** $\Delta_{LC-cro}$ (dark grey bars in Fig. 4B). The presence of iron/metals and related descendant structural parameters

(like iron nuclearity) play a pivotal role in fibre toxicity because they govern the primary production of cyto-/geno-toxic oxidant species like the hydroxyl radical $HO^{\bullet}$, created via the Fenton reaction $Fe^{2+} + H_2O_2 \rightarrow Fe^{3+} + OH^- + HO^{\bullet}$ (Hardy and Aust, 1995). As reported in Shukla et al. (2003), these reactions are not related only to the total iron content although epidemiological studies indicate that iron-containing asbestos fibres appear more carcinogenic (Toyokuni, 2023). The presence of specific iron catalytic sites at the surface of both chrysotile and crocidolite become active in free radical generation only when present at specific crystallographic sites in a definite oxidation and coordination state. The produced reactive oxygen species (ROS) are responsible for oxidative stress and chronic inflammation (Hardy and Aust, 1995; Fubini and Mollo, 1995; Shukla et al., 2003) although the mechanism is different for chrysotile and crocidolite. Chrysotile is not biodurable and when it dissolves, the metals hosted in its structure are released, mimicking the so-called 'Trojan horse effect' known to explain the toxicity of nanoparticles (Studer et al., 2010; Gualtieri et al., 2019b). The high dissolution rate (1,12), with the release of transition metals and magnesium explain the potent haemolytic activity of chrysotile with respect to crocidolite (Nagai et al., 2011). Crocidolite instead is biodurable and its surface represents a bioavailable perpetual metals' pool (Gualtieri et al., 2019a). Following the model proposed by Ghio et al. (2023), these metals, namely iron, made bioavailable from the fibres are chelated at the surface of the fibres themselves as the negatively charged silanol groups at the surface of the fibres complex and adsorb the metals. Iron complexation at the surface of the fibres prompts an early cellular iron homeostasis disruption which becomes much more intense later with the supply of biological iron (Ghio, 2009). Epithelial lung cells and macrophages (due to frustrated phagocytosis) exposed to iron can rapidly increase the expression of ferritin protein. Biological iron continues to be supplied and complex at the surface of the fibres and this functional deficiency of iron magnifies the iron homeostasis disruption responsible for generalized inflammation, oxidative stress, expression of importers, activation of kinases/phosphatases and transcription factors (Ghio et al., 2023). We believe that extracellular iron supplied by the fibres should have a role at least in the early cellular iron homeostasis disruption. Ghio et al. (2023) instead claim that fibres' structural iron has a negligible biological effect. Despite the role of fibres' structural iron, the model of carcinogenesis based on "iron deficiency" due to homeostasis disruption postulated by Ghio (2009) apparently has an alternative in the model of "iron excess" based on ferroptosis, a regulated cellular necrosis dependent on catalytic iron followed by lipid peroxidation assumed by Toyokuni (2013, 2019). The two models

actually share the same concept of disruption of iron homeostasis rupture from two different perspectives: Ghio (2009) focuses on the (excessive) depletion of biological functional iron in the body that migrates and is sequestered at the surface of the fibres while Toyokuni (2013, 2023) focuses on the (excessive) concentration itself of biological functional iron at the surface of the fibres.

Fig. 5 summarizes the fibre parameters more relevant in activating the KCs that discriminate chrysotile from crocidolite. Except for length that marks chrysotile with long fibres (**LC**), relevant fibre parameters contributing to the KCs for chrysotile are: surface area (1,7) and the dissolution rate (1,12) with the related velocity of iron release (1,13) and velocity of release of metals, like Cr, Ni and Mn (Gualtieri et al., 2019b; Mirata et al., 2022; Almonti et al., 2024) (1,15). For crocidolite, relevant fibre parameters contributing to the KCs are: fibre length (1,1), iron content (1,8) and related parameters ferrous iron content (1,9) and iron nuclearity (1,10), content of metals other than iron (1,11) and zeta potential (1,16).

Our model suggests that for both chrysotile and crocidolite fibres, iron and eventually other transition metals are major parameters of the carcinogens, as originally proposed in the early works on iron toxicity/pathogenicity by Hardy and Aust (1995), Fubini and Mollo (1995), Fubini, 1997, and Aust et al. (2000). We acknowledge the credit of prof. Bice Fubini, who had the brilliant intuition almost 30 years ago to recognize iron as a major contributor to the toxicity of mineral fibres and paved the way for the neutralization of its surface activity *in vivo* with the help of chelating substances (Fubini et al., 1995). Following that concept and the subsequent research lines that flowed from that original idea, we support the prevention therapies aimed at keeping iron homeostasis even in the early steps of the process when only structural iron from the fibres is made available:

– decreasing the iron stores by iron chelators (Hatcher et al., 2009; Toyokuni, 2019);
– phlebotomy once a month (Toyokuni, 2019);
– control of the ferroptosis cell death process (Claudio-Ares et al., 2024; Foroutan et al., 2024);
– promote iron depletion, using iron mimetics, or targeting the overexpressed iron homeostasis proteins in cancer cells, following one of the earliest approaches involved using anti-TFR1 (CD71) antibodies to inhibit cancer growth by restricting the iron uptake through the TF-TFR1 pathway (Rishi et al., 2021);
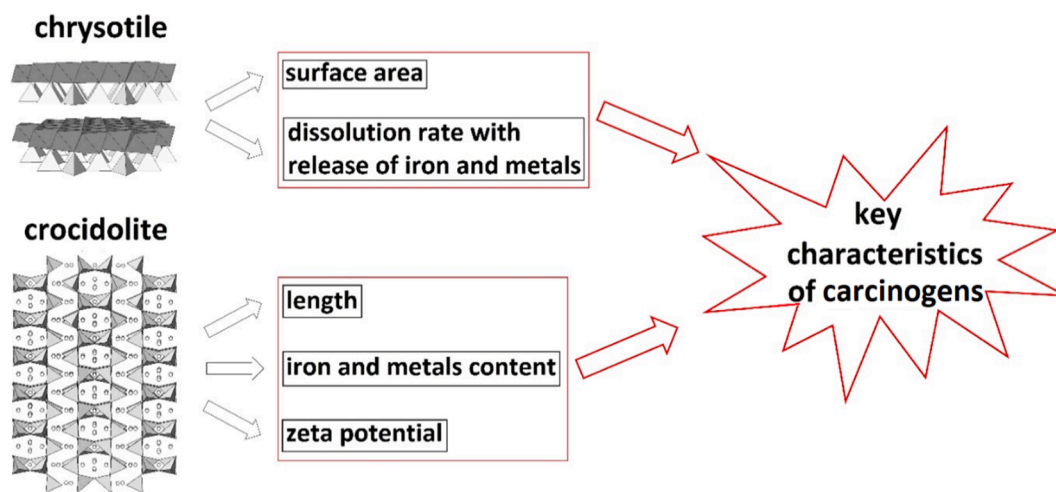


**Fig. 5.** Diagram showing the fibre characteristics that most actively contribute to the KCs for chrysotile (surface area (1,7); the dissolution rate (1,12) with the related velocity of iron release (1,13) and velocity of release of metals (1,15)) and for crocidolite (fibre length (1,1); iron content (1,8) with the related parameters ferrous iron content (1,9) and iron nuclearity (1,10); content of metals other than iron (1,11); zeta potential (1,16)).

- use of extracellular micro-vesicles and exosomes (Munson and Shukla, 2022) to remove iron excess out of the cells exposed to ferroptosis stimuli (Toyokuni et al., 2023; Rahimian et al., 2024).

These therapies can be integrated with:

- preventive anti-inflammatory treatment with aspirin helpful for the prevention of asbestos induced mesothelioma in animal models (Yang et al., 2015);
- dietary depletion joined with chelator therapy (Ghio, 2009).

Because some differences in the fibre parameters that stimulate carcinogenicity parameters are observed for chrysotile and crocidolite (Fig. 5), is it possible to speculate on future fibre-selective prevention therapies. Following the major prevention strategy based on iron chelators (Hatcher et al., 2009; Toyokuni, 2019), the active iron-targeting molecules should work when the fibres are still in the extracellular environment, at neutral pH. For the positive surface of the chrysotile fibres, chelation and inactivation of iron should be accomplished with a mix of deferasirox $C_{21}H_{15}N_3O_4$ (DFX) and deferoxamine $C_{25}H_{48}N_6O_8$ (DFO), both chemically attracted by silica positive surfaces (Kumar et al., 2013; Taghavi et al., 2016). DFX can chelate both $Fe^{3+}$ and $Fe^{2+}$ (Piolatto et al., 2021) while DFO preferentially chelates $Fe^{3+}$ ions (see for example, Liang et al., 2009). For the negative surface of crocidolite, chelation and inactivation of iron can be effectively accomplished with deferiprone $C_7H_9NO_2$ (DFP), chemically attracted by silica negative surfaces and active for both $Fe^{2+}$ and $Fe^{3+}$ ions (see for example, Timoshnikov et al., 2015) with $Fe^{3+} > Fe^{2+}$ (Liu and Hider, 2002). To specifically target asbestos fibres, all characterised by high $SiO_2$ content, iron-chelators may be combined with molecules known for their ability to recognize and bind to silica surfaces like silica-binding peptides, antibodies, aptamers, and small molecules/polymers that can be designed with specific motifs or functional groups with an affinity for silica surfaces (see for example, Ikeda and Kuroda, 2011). Peptides are especially suited to bind silica surfaces. Among them, peptides containing either aspartic acid $(C_4H_7NO_4)$ (Asp) or lysine $(C_6H_{14}N_2O_2)$ could specifically target chrysotile positive surfaces or crocidolite negative surfaces, respectively (Guo and Holland, 2014). The design of these selective peptides could be accomplished with the aid of genetically engineered peptides for inorganics (GEPI) protocols (Tamerler and Sarikaya, 2009). The possibility to use biocompatible and biodegradable nanocarriers (engineering precision nanoparticles for drug delivery) (Mitchell et al., 2021) or synthetic zeolites/mesoporous materials (Maleki et al., 2020) as vectors should be considered. Fig. 6 is a sketch of an ideal nanocarrier with a complex of peptides and iron chelators especially designed for chrysotile (a) and crocidolite (b), respectively.

## Conclusions

A commercial chrysotile, with short ($\leq 5$ μm) and long ($>5$ μm) fibres, the carcinogenic standard UICC crocidolite and the non-carcinogenic standard wollastonite NYAD G were tested *in vitro* to collect data on the KCs. The application of the FPTI model (Gualtieri, 2021) to the *in vitro* data made it possible to assess the fibre parameters responsible for the activation of the KCs for each mineral fibre. We found that some fibre parameters like the crystal habit and density are not involved in the activation of the carcinogenicity parameters because they mostly affect the viability of the fibres to reach the lung environment but not the interaction with the cells and possible activation of adverse effects related to carcinogenesis. The major fibre parent parameters contributing to the KCs are: length, iron content, content of metals, dissolution rate, and zeta potential while descendant parameters are: surface area, ferrous iron content, iron nuclearity, velocity of iron release, and velocity of release of metals. Besides fibre length for chrysotile with long fibres, major fibre parameters contributing to the KCs for chrysotile are the surface area and the dissolution rate with the
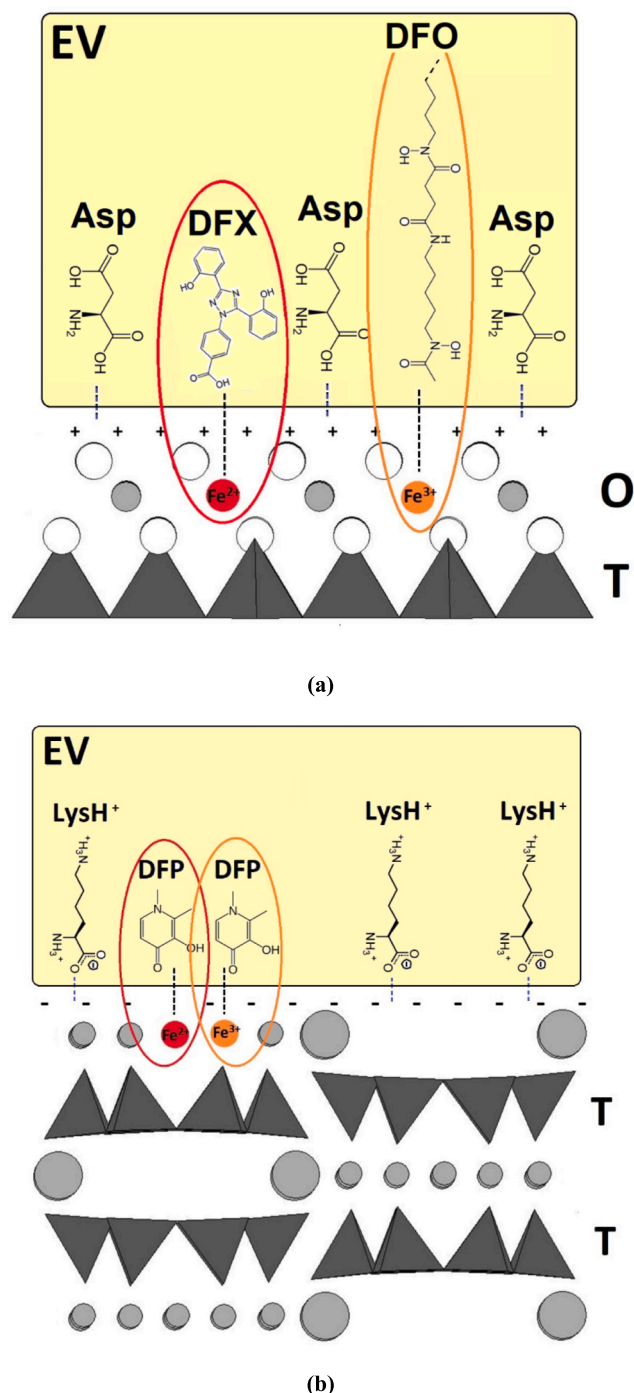


**(a)**



**(b)**

**Fig. 6.** An ideal surface-engineered nanocarrier (EV) with specific peptides and iron chelators especially designed for chrysotile (a) and crocidolite (b). In (a), a mix of DFX and DFO targets the positive surface, with DFX that can chelate $Fe^{2+}$ and DFO that preferentially chelates $Fe^{3+}$. The anchorage of the complex to the silica chrysotile surface is driven by Asp. In (b), DFP targets the negative crocidolite surface and chelates both $Fe^{3+}$ and $Fe^{2+}$. The anchorage of the complex to the silica crocidolite surface is driven by lysine. The tetrahedral (T) layers host Si atoms. The octahedral (O) layer in chrysotile hosts namely Mg atoms with minor $Fe^{2+}$ and $Fe^{3+}$. The exposed layer in crocidolite hosts $Fe^{2+}$ and $Fe^{3+}$ in the octahedrally coordinated sites and $Na^+$ in the cubic antiprismatic site.

related velocity of iron release and velocity of release of metals. For crocidolite, they are the fibre length, iron/metals content and related parameters ferrous iron content and iron nuclearity, and zeta potential.

In the time of precision medicine (Ye et al., 2019), our results can be a starting point for developing personalized cancer prevention strategies as long as it is known the nature of the fibre the patient was exposed to. Among prevention therapies, those aimed at inhibiting biological iron overload are probably the most promising (Hatcher et al., 2009; Toyokuni, 2019). These strategies can also be employed as a preventive measure by chelating the iron released at the surface from the fibres and inhibiting the initial stages of iron accumulation.

A future design of fibre-selective prevention therapies should target the fibres with surface-engineered nanocarriers with active complexes when they are still in the extracellular environment. For chrysotile, a mix of DFX and DFO iron chelators to target the positive surface is proposed. The anchorage of the complex to the silica chrysotile surface may be driven by aspartic acid. For crocidolite, DFP to target the negative crocidolite surface and chelates both $Fe^{2+}$ and $Fe^{3+}$ with anchorage of the complex to the silica crocidolite surface favoured by lysine.

At the moment, we can only deliver a speculative sound model for the prevention therapy. To finalize the model, we need to perform *ab initio* modelling for surface interaction with density functional theory (DFT) (see for example, Ahmad et al, 2020) to find the best chelating system and understand its surface interaction with the fibres. Moreover, the search for the best silicate-targeting peptides biomolecular composites taking advantage of the GEPIs database (Tamerler et al., 2009), is required. Different prevention strategies should be planned for other carcinogenic fibres like the zeolite erionite whose iron-content is low and due to impurities, mostly concentrated at the surface of the fibres (Gualtieri et al., 2016).

## CRediT authorship contribution statement

**Alessandro F. Gualtieri:** Resources, Data curation, Formal analysis, Investigation, Methodology, Writing – original draft, Writing – review & editing. **Erika Ferrari:** Investigation, Writing – review & editing. **Luca Rigamonti:** Investigation, Writing – review & editing. **Barbara Ruozi:** Methodology, Writing – review & editing. **Serena Mirata:** Data curation. **Vanessa Almonti:** Data curation. **Mario Passalacqua:** Data curation, Writing – review & editing. **Stefania Vernazza:** Data curation. **Silvia Di Valerio:** Data curation. **Giovanni Tossetta:** Data curation. **Salvatore Vaiasicca:** Data curation. **Antonio D. Procopio:** Data curation. **Francesca Fazioli:** Data curation. **Daniela Marzioni:** Data curation, Investigation, Methodology, Writing – review & editing. **Armanda Pugnaloni:** Data curation, Investigation, Methodology, Writing – review & editing. **Sonia Scarfì:** Data curation, Investigation, Methodology, Writing – review & editing.

## Funding

## Declaration of competing interest

The authors declare that they have no known competing financial interests or personal relationships that could have appeared to influence the work reported in this paper.

## Appendix A. Supplementary data

Supplementary data to this article can be found online at https://doi.org/10.1016/j.crtox.2024.100202.

## Data availability

Data will be made available on request.

## References

Ahmad, R., Ali, Z., Khan, A.A., Rehman, N.U., 2020. Terbium extraction by functionalized surface: experimental and DFT approach. Adsorption 26 (1), 117–125.

Almonti, V., Vernazza, S., Mirata, S., Tirendi, S., Passalacqua, M., Gualtieri, A.F., Di Giuseppe, D., Scarfì, S., Bassi, A.M., 2024. Toxicity and inflammatory potential of mineral fibres: the contribute of released soluble metals versus cell contact direct effects. J. Appl. Toxicol. 11. https://doi.org/10.1002/jat.4610.

Anttila, S., Boffetta, P. (Eds.), 2020. Occupational cancers. Springer Nature, pp. 640. ISBN : 978-3-030-30765-3.

Aust, E.A., Lund, L.G., Chao, C.C., Park, S.H., Fang, R., 2000. Role of iron in the cellular effects of asbestos. Inhal. Toxicol. 12 (sup3), 75–80.

Borchert, S., Suckrau, P.M., Wessolly, M., Mairinger, E., Hegedus, B., Hager, T., Herold, T., Eberhardt, W.E.E., Wohlschlaeger, J., Aigner, C., Bankfalvi, A., Schmid, K.W., Walter, R.F.H., Mairinger, F.D., 2019. Screening of pleural mesothelioma cell lines for kinase activity may identify new mechanisms of therapy resistance in patients receiving platin-based chemotherapy. J. Oncol. 2902985. https://doi.org/10.1155/2019/2902985.

Brambilla, M., Talmon, M., Canzano, P., Fresu, L.G., Brunelleschi, S., Tremoli, E., Camera, M., 2022. Different contribution of monocyte- and platelet-derived microvesicles to endothelial behavior. Int. J. Mol. Sci. 23 (9), 4811. https://doi.org/10.3390/ijms23094811.

Carbone, M., Adusumilli, P.S., Alexander Jr, H.R., Baas, P., Bardelli, F., Bononi, A., Bueno, R., Felley-Bosco, E., Galateu-Salle, F., Jablons, D., Mansfield, A.S., Minaai, M., de Perrot, M., Pesavento, P., Rusch, V., Severon, D.T., Taioli, E., Tsao, A., Woodard, G., Yang, H., Zauderer, G., Pass, H.I., 2019. Mesothelioma: scientific clues for prevention, diagnosis, and therapy. Ca-Cancer J. Clin. 69, 402–429.

Cardile, V., Lombardo, L., Belluso, E., Panico, A., Capella, S., Balazy, M., 2007. Toxicity and carcinogenicity mechanisms of fibrous antigorite. Int. J. Environ. Res. Public Health 4 (1), 1–9. https://doi.org/10.3390/ijerph2007010001.

Chanput, W., Mes, J.J., Wichers, H.J., 2014. THP-1 cell line: an in vitro cell model for immune modulation approach. Intern Immunopharmacol. 23, 37–45.

Claudio-Ares, O., Luciano-Rodríguez, J., Del Valle-González, Y.L., Schiavone-Chamorro, S.L., Pastor, A.J., Rivera-Reyes, J.O., Metzler, C.L., Domínguez-Orona, L. M., Vargas-Pérez, B.L., Skouta, R., Tinoco, A.D., 2024. Exploring the use of intracellular chelation and non-iron metals to program ferroptosis for anticancer application. Inorganics 12 (1), 26. https://doi.org/10.3390/inorganics12010026.

Cooke, W.E., 1924. Fibrosis of the lungs due to inhalation of asbestos dust. Br. Med. J. 2, 147.

Di Giuseppe, D., Zoboli, A., Nodari, L., Pasquali, L., Sala, O., Ballirano, P., Malferrari, D., Raneri, S., Hanuskova, M., Gualtieri, A.F., 2021a. Characterization and assessment of the potential toxicity/pathogenicity of Russian commercial chrysotile. Am. Mineral. 106, 1606–1621.

Di Giuseppe, D., Scognamiglio, V., Malferrari, D., Nodari, L., Pasquali, L., Lassinantti Gualtieri, M., Scarfì, S., Mirata, S., Tessari, U., Hanuskova, M., Gualtieri, A.F., 2021b. Characterization of fibrous wollastonite NYAD G in view of its use as negative standard for *in vitro* toxicity tests. Minerals 11 (12), 1378.

Dobrzynska, M., Napierala, M., Florek, E., 2020. Flavonoid nanoparticles: a promising approach for cancer therapy. Biomolecules 10 (9), 1268. https://doi.org/10.3390/biom10091268.

Donaldson, K., Murphy, F.A., Duffin, R., Poland, C.A., 2010. Asbestos, carbon nanotubes and the pleural mesothelium: a review of the hypothesis regarding the role of long fibre retention in the parietal pleura, inflammation and mesothelioma. Part. Fibre Toxicol. 7, 5–22.

Dunningan, J., 1984. Biological effects of fibers: Stanton's hypothesis revisited. Environ. Health Perspect. 57, 333–337.

Foroutan, Z., Butler, A.E., Zengin, G., Sahebkar, A., 2024. Curcumin and ferroptosis: a promising target for disease prevention and treatment. Cell Biochem. Biophys. 1–7.

Fubini, B., 1997. Surface reactivity in the pathogenic response to particulates. Environ. Health Perspect. 105 (suppl 5), 1013–1020.

Fubini, B., Mollo, L., Giamello, E., 1995. Free radical generation at the solid/liquid interface in iron containing minerals. Free Radic. Res. 23 (6), 593–614.

Fubini, B., Mollo, L., 1995. Role of iron in the reactivity of mineral fibers. Toxicol. Lett. 82, 951–960.

Ghio, A.J., 2009. Disruption of iron homeostasis and lung disease. Biochim. Biophys. Acta (BBA)-Gen. Sub. 1790 (7), 731–739.

Ghio, A.J., Stewart, M., Sangani, R.G., Pavlisko, E.N., Roggli, V.L., 2023. Asbestos and iron. Int. J. Mol. Sci. 24 (15), 12390. https://doi.org/10.3390/ijms241512390.

Goodman, J.E., Lynch, H.N., Rhomberg, L.R., 2018, Letter to the editor re: Guyton et al. (2018), 'Application of the key characteristics of carcinogens in cancer hazard identification. Carcinogenesis, 39(8), 1089–1090.

Gualtieri, A.F., 2017. Mineral Fibres: Crystal Chemistry, Chemical-Physical Properties, Biological Interaction and Toxicity. European Mineralogical Union-EMU Notes in Mineralogy, London.

Gualtieri, A.F., 2018. Towards a quantitative model to predict the toxicity/pathogenicity potential of mineral fibers. Toxicol. Appl. Pharm. 361, 89–98.

Gualtieri, A.F., 2021. Bridging the gap between toxicity and carcinogenicity of mineral fibres by connecting the fibre crystal-chemical and physical parameters to the key characteristics of cancer. Curr. Res. Toxicol. 2, 42–52.

Gualtieri, A.F., 2023. Journey to the centre of the lung. The perspective of a mineralogist on the carcinogenic effects of mineral fibres in the lungs. J. Hazard. Mater. 442, 130077. https://doi.org/10.1016/j.jhazmat.2022.130077.

Gualtieri, A.F., Gandolfi, N.B., Pollastri, S., Pollok, K., Langenhorst, F., 2016. Where is iron in erionite? A multidisciplinary study on fibrous erionite-Na from Jersey (Nevada, USA). Sci. Rep. 6 (1), 37981.

Gualtieri, A.F., Pollastri, S., Gandolfi, N.B., Lassinantti Gualtieri, M., 2018. *In vitro* acellular dissolution of mineral fibres: A comparative study. Sci. Rep. 8 (1), 1–12.

Gualtieri, A.F., Andreozzi, G.B., Tomatis, M., Turci, F., 2019a. Iron from a geochemical viewpoint. Understanding toxicity/pathogenicity mechanisms in iron-bearing minerals with a special attention to mineral fibers. Free Radical. Bio. Med. 133, 21–37.

Gualtieri, A.F., Lusvardi, G., Zoboli, A., Di Giuseppe, D., Lassinantti Gualtieri, M., 2019b. Biodurability and release of metals during the dissolution of chrysotile, crocidolite and fibrous erionite. Environ. Res. 171, 550–557.

Gualtieri, A.F., Leoncini, M., Rinaldi, L., Zoboli, A., Di Giuseppe, D., 2021. WebFPTI: A tool to predict the toxicity/pathogenicity of mineral fibres including asbestos. Earth Sci. Inf. 14 (4), 2401–2409.

Gualtieri, A.F., Mirata, S., Almonti, V., Bassi, A.M., Meo, C., Scarfì, S., Zapparoli, M., Armeni, T., Cianfruglia, L., Marzioni, D., Fantone, S., Tossetta, G., Stipa, P., Laudadio, E., Sabbatini, M., Minnelli, C., Di Valerio, V., Vaiasicca, S., Procopio, A.D., Pugnaloni, A., 2023. *In vitro* toxicity of short vs. long chrysotile fibres. Periodico Di Mineralogia 92 (2), 203–222.

Guo, C., Holland, G.P., 2014. Investigating lysine adsorption on fumed silica nanoparticles. J. Phys. Chem. C 118 (44), 25792–25801.

Hardy, J.A., Aust, A.E., 1995. Iron in asbestos chemistry and carcinogenicity. Chem. Rev. 95, 97–118.

Harris, R.L. Timbrell, V., 1977. Relation of alveolar deposition to the diameter and length of glass fibres. In: Proceedings of the Inhaled Particles IV: Proceedings of an International Symposium Organized by the British Occupational Hygiene Society, Edinburgh. Pergamon Press Oxford, 411 pp.

Hatcher, H.C., Singh, R.N., Torti, F.M., Torti, S.V., 2009. Synthetic and natural iron chelators: therapeutic potential and clinical use. Future Med. Chem. 1 (9), 1643–1670.

Holmes, D., 2013. IARC in the dock over ties with asbestos industry. Lancet 381 (9864), 359–361.

Hume, L.A., Rimstidt, J.D., 1992. The biodurability of chrysotile asbestos. Am. Mineral. 77 (9–10), 1125–1128.

Ikeda, T., Kuroda, A., 2011. Why does the silica-binding protein "Si-tag" bind strongly to silica surfaces? Implications of conformational adaptation of the intrinsically disordered polypeptide to solid surfaces. Colloids Surf. B Biointerf. 86 (2), 359–363.

Ito, F., Kato, K., Yanatori, I., Murohara, T., Toyokuni, S., 2021. Ferroptosis-dependent extracellular vesicles from macrophage contribute to asbestos-induced mesothelial carcinogenesis through loading ferritin. Redox Biol. 47, 102174. https://doi.org/10.1016/j.redox.2021.102174.

Jiang, L., Akatsuka, S., Nagai, H., Chew, S.H., Ohara, H., Okazaki, Y., Yamashita, Y., Yoshikawa, Y., Yasui, H., Ikuta, K., Sasaki, K., Kohgo, Y., Hirano, S., Shinohara, Y., Kohyama, N., Takahashi, T., Toyokuni, S., 2012. Iron overload signature in chrysotile-induced malignant mesothelioma. J. Pathol. 228 (3), 366–377.

Krewski, D., Bird, M., Al-Zoughool, M., Birkett, N., Billard, M., Milton, B., Rice, J.M., Grosse, Y., Cogliano, V.J., Hill, M.A., Baan, R.A., Little, J., Zielinski, J.M., 2019. Key characteristics of 86 agents known to cause cancer in humans. J. Tox. Env. Health Part B 22, 244–263.

Kumar, R., Barakat, M.A., Daza, Y.A., Woodcock, H.L., Kuhn, J.N., 2013. EDTA functionalized silica for removal of Cu (II), Zn (II) and Ni (II) from aqueous solution. J. Colloid Interface Sci. 408, 200–205.

Laurent, A., Abdel-Sayed, P., Hirt-Burri, N., Scaletta, C., Michetti, M., de Buys Roessingh, A., Raffoul, W., Applegate, L.A., 2021. Evolution of diploid progenitor lung cell applications: from optimized biotechnological substrates to potential active pharmaceutical ingredients in respiratory tract regenerative medicine. Cells 10 (10), 2526. https://doi.org/10.3390/cells10102526.

Li, M., Gunter, M.E., Fukagawa, N.K., 2012. Differential activation of the inflammasome in THP-1 cells exposed to chrysotile asbestos and Libby "Six-Mix" amphiboles and subsequent activation of BEAS-2B cells. Cytokine 60 (3), 718–730. https://doi.org/10.1016/j.cyto.2017.01.011.

Liang, C., Liang, C.P., Chen, C.C., 2009. pH dependence of persulfate activation by EDTA/Fe (III) for degradation of trichloroethylene. J. Contam. Hydrol. 106 (3–4), 173–182.

Liddell, F.D.K., Miller, K., 1991. Mineral Fibers and Health. CRC Press.

Liu, Z.D., Hider, R.C., 2002. Design of iron chelators with therapeutic application. Coord. Chem. Rev. 232 (1–2), 151–171.

Maki, Y., Nishimura, Y., Toyooka, S., Soh, J., Tsukuda, K., Shien, K., Furukawa, M., Muraoka, T., Ueno, T., Tanaka, N., Yamamoto, H., Asano, H., Maeda, M., Kumagai-Takei, N., Lee, S., Matsuzaki, H., Otsuki, T., Miyoshi, S., 2016. The proliferative effects of asbestos-exposed peripheral blood mononuclear cells on mesothelial cells. Oncol Lett. 11 (5), 3308–3316. https://doi.org/10.3892/ol.2016.4412.

Maleki, A., Shahbazi, M.A., Alinezhad, V., Santos, H.A., 2020. The progress and prospect of zeolitic imidazolate frameworks in cancer therapy, antibacterial activity, and biomineralization. Adv. Healthc. Mater. 9 (12), 2000248.

Mirata, S., Almonti, V., Di Giuseppe, D., Fornasini, L., Raneri, S., Vernazza, S., Bersani, D., Gualtieri, A.F., Bassi, A.M., Scarfì, S., 2022. The acute toxicity of mineral Fibres: a systematic in vitro study using different THP-1 macrophage phenotypes. Int. J. Mol. Sci. 23 (5), 2840. https://doi.org/10.3390/ijms23052840.

Mirata, S., Bassi, A.M., Almonti, V., Tirendi, S., Vernazza, S., Fornasini, L., Raneri, S., Bersani, D., Passalacqua, M., Gualtieri, A.F., Scarfì, S., 2023. Cytotoxic and pro-inflammatory early effects of mineral fibres on human alveolar epithelial and immune cells. Periodico Di Mineralogia 92 (2), 223–229.

Mitchell, M.J., Billingsley, M.M., Haley, R.M., Wechsler, M.E., Peppas, N.A., Langer, R., 2021. Engineering precision nanoparticles for drug delivery. Nat. Rev. Drug Discov. 20 (2), 101–124. https://doi.org/10.1038/s41573-020-0090-8.

Moore, D.S., McCabe, G.P., 1999. Introduction to the Practice of Statistics, third ed. W.H. Freeman, New York.

Mossman, B.T., Gualtieri, A.F., 2020. Lung cancer: Mechanisms of carcinogenesis by asbestos. In: Anttila, S., Boffetta, P. (Eds.), Occupational Cancers. Springer, pp. 239–256.

Munson, P., Shukla, A., 2022. Potential Roles of Exosomes in the Development and Detection of Malignant Mesothelioma: An Update. Int. J. Mol. Sci. 23 (23), 15438.

Nagai, H., Ishihara, T., Lee, W.H., Ohara, H., Okazaki, Y., Okawa, K., Toyokuni, S., 2011. Asbestos surface provides a niche for oxidative modification. Cancer Sci. 102 (12), 2118–2125.

Pavlisko, E.N., Sporn, T.A., 2013. Mesothelioma. In: Oury, T.D., Sporn, T.A., Roggli, V.L. (Eds.), Pathology of Asbestos-Associated Diseases. Springer, pp. 81–140.

Piolatto, A., Berchialla, P., Allegra, S., De Francia, S., Ferrero, G.B., Piga, A., Longo, F., 2021. Pharmacological and clinical evaluation of deferasirox formulations for treatment tailoring. Sci. Rep. 11 (1), 12581.

Pollastri, S., Gualtieri, A.F., Lassinantti Gualtieri, M., Hanuskova, M., Cavallo, A., Gaudino, G., 2014. The zeta potential of mineral fibres. J. Hazard. Mater. 276, 469–479.

Pollastri, S., D'Acapito, F., Trapananti, A., Colantoni, I., Andreozzi, G.B., Gualtieri, A.F., 2015. The chemical environment of iron in mineral fibres. A combined X-ray absorption and Mössbauer spectroscopic study. J. Hazard. Mater. 298, 282–293.

Rahimian, S., Najafi, H., Afzali, B., Doroudian, M., 2024. Extracellular vesicles and exosomes: novel insights and perspectives on lung cancer from early detection to targeted treatment. Biomedicines 12 (1), 123.

Rebecca, C.E., Garle, M.J., Fry, J.R., 2000. Glutathione depletion in a liver microsomal assay as an in vitro biomarker for reactive metabolite formation. Biomarkers 5, 285–294.

Rishi, G., Huang, G., Subramaniam, V.N., 2021. Cancer: the role of iron and ferroptosis. Int. J. Biochem. Cell Biol. 141, 106094.

Scognamiglio, V., Di Giuseppe, D., Lassinantti, G.M., Tomassetti, L., Gualtieri, A.F., 2021. A systematic study of the cryogenic milling of chrysotile asbestos. Appl. Sci. 11, 4826.

Shukla, A., Gulumian, M., Hei, T.K., Kamp, D., Rahman, Q., Mossman, B.T., 2003. Multiple roles of oxidants in the pathogenesis of asbestos-induced diseases. Free Radical Biol. Med. 34, 1117–1129.

Smith, M.T., Guyton, K.Z., Gibbons, C.F., Fritz, J.M., Portier, C.J., Rusyn, I., DeMarini, D. M., Caldwell, J.C., Kavlock, R.J., Lambert, P.F., Hecht, S.S., Bucher, J.R., Stewart, B. W., Baan, R.A., Cogliano, V.J., Straif, K., 2016. Key characteristics of carcinogens as a basis for organizing data on mechanisms of carcinogenesis. Environ. Health Persp. 124, 713–721.

Smith, M.T., Guyton, K.Z., Kleinstreuer, N., Borrel, A., Cardenas, A., Chiu, W.A., Felsher, D.W., Gibbons, C.F., Goodson, W.H., Houck, K.A., Kane, A.B., La Merrill, M. A., Lebrec, H., Lowe, L., McHale, C.M., Minocherhomji, S., Rieswijk, L., Sandy, M.S., Sone, H., Wang, A., Zhang, L., Zeise, L., Fielden, M., 2020. The key characteristics of carcinogens: relationship to the hallmarks of cancer, relevant biomarkers, and assays to measure them. Cancer Epidemiol. Biomark. Prev. 29 (10), 1887–1903.

Stanton, M.F., Layard, M., Tegeris, A., Miller, E., May, M., Morgan, E., Smith, A., 1981. Relation of particle dimension to carcinogenicity in amphibole asbestoses and other fibrous minerals. J. Natl. Cancer Inst. 67, 965–975.

Studer, A.M., Limbach, L.K., Van Duc, L., Krumeich, F., Athanassiou, E.K., Gerber, L.C., Moch, H., Stark, W.J., 2010. Nanoparticle cytotoxicity depends on intracellular solubility: comparison of stabilized copper metal and degradable copper oxide nanoparticles. Toxicol. Lett. 197 (3), 169–174.

Taghavi, F., Gholizadeh, M., Saljooghi, A.S., 2016. Deferasirox loaded on fumed silica nanoparticles used in cancer treatment. New J. Chem. 40 (3), 2696–2703.

Tamerler, C., Sarikaya, M., 2009. Molecular biomimetics: nanotechnology and bionanotechnology using genetically engineered peptides. Philos. Trans. R. Soc. A Math. Phys. Eng. Sci. 367 (1894), 1705–1726.

Timoshnikov, V.A., Kobzeva, T.V., Polyakov, N.E., Kontoghiorghes, G.J., 2015. Inhibition of $Fe^{2+}$-and $Fe^{3+}$-induced hydroxyl radical production by the iron-chelating drug deferiprone. Free Radical Biol. Med. 78, 118–122.

Toyokuni, S., 2013. Iron overload as a major targetable pathogenesis of asbestos-induced mesothelial carcinogenesis. Redox Rep. 19, 1–7.

Toyokuni, S., 2019. Iron addiction with ferroptosis-resistance in asbestos-induced mesothelial carcinogenesis: toward the era of mesothelioma prevention. Free Radical Biol. Med. 133, 206–215.

Toyokuni, S., 2023. Commentary on "Mechanisms of asbestos-induced carcinogenesis" published in 2009. Nagoya J. Med. Sci. 85, 13–15.

Toyokuni, S., Kong, Y., Katabuchi, M., Maeda, Y., Motooka, Y., Ito, F., Yanatori, I., 2023. Iron links endogenous and exogenous nanoparticles. Arch. Biochem. Biophys. 745, 109718.

Vargha, A., Delaney, H.D., 1998. The Kruskal-Wallis test and stochastic homogeneity. J. Educ. Behav. Stat. 23 (2), 170–192.

Who, 1997. Determination of Airborne Fibre Number Concentrations; A Recommended Method, By Phase-Contrast Optical Microscopy (Membrane Filter Method). Switzerland, World Health Organization, Geneva, p. 53.

Yang, H., Pellegrini, L., Napolitano, A., Giorgi, C., Jube, S., Preti, A., Jennings, C.J., De Marchis, F., Flores, E.G., Larson, D., Pagano, I., Tanji, M., Powers, A., Kanodia, S., Gaudino, G., Pastorino, S., Pass, H.I., Pinton, P., Bianchi, M.E., Carbone, M., 2015. Aspirin delays mesothelioma growth by inhibiting HMGB1-mediated tumor progression. Cell Death Dis. 6 (6), e1786.

Ye, L., Ma, S., Robinson, B.W., Creaney, J., 2019. Immunotherapy strategies for mesothelioma–the role of tumor specific neoantigens in a new era of precision medicine. Expert Rev. Respir. Med. 13 (2), 181–192.

Yeh, H.C., Phalen, R.F., Raabe, O.G., 1976. Factors influencing the deposition of inhaled particles. Environ. Health Perspect. 15, 147–156.

Zbeeb, H., Baldini, F., Zeaiter, L., Vergani, L., 2024. The anti-inflammatory potential of an ethanolic extract from sarcopoterium spinosum fruits for protection and/or counteraction against oxidative stress in dysfunctional endothelial cells. Int. J. Mol. Sci. 25 (3), 1601. https://doi.org/10.3390/ijms25031601.